

Memory of Surface Patterns in Mixed Polymer Brushes: Simulation and Experiment[†]

Svetlana Santer,^{*,‡,⊥} Alexey Kopyshov,[‡] Jörn Donges,[‡] Jürgen Rühle,[‡] Xueguang Jiang,[§] Bin Zhao,[§] and Marcus Müller^{*,||}

Department of Microsystems Engineering (IMTEK), University of Freiburg, Georges-Koehler-Allee 103, D-79110 Freiburg, Germany, Department of Chemistry, University of Tennessee, Knoxville, Tennessee 37996, and Institut für Theoretische Physik, Georg-August Universität, D-37077 Göttingen, Germany

Received October 8, 2006. In Final Form: October 30, 2006

The correlation between the morphology of mixed polymer brushes and fluctuations of the grafting points is investigated by single-chain-in-mean-field simulations and experiments. The local topography of two types of mixed polystyrene–polymethylmethacrylate (PS–PMMA) brushes that differ in their modes of attachment has been studied during repeated microphase separation into laterally structured and homogeneous morphologies upon changing solvents. In the first type of brush (conventional), each of the surface-attached initiator groups starts the growth of either a PS or a PMMA chain in a random fashion. In the second case (Y-shaped mixed brushes), two chains of different types are attached to the same anchor group on the substrate. Whereas in the first case statistical fluctuations of the chemical composition occur on a local scale, such composition fluctuations are strongly suppressed in the latter case. The microphase-separated morphology is similar in both cases, but Y-shaped brushes exhibit a significantly weaker domain memory than do conventional PS–PMMA mixed brushes. The results of the experiment are compared with simulations, and a simple phenomenological argument and qualitative agreement are found. The observations demonstrate that small fluctuations in the grafting points are amplified by the microphase separation and nucleate the location of the domains in the mixed brush.

Introduction

Mixed polymer brushes consisting of two homopolymers being covalently attached with one end to a solid substrate have attracted abiding interest^{1–20} because of their ability to switch properties

such as the surface energy (hydrophilicity/hydrophobicity) and/or surface topography in response to changes of their environment. Because of the immobility of the grafting points, macroscopic demixing is impossible. Instead, domains on a nanometer scale form (termed microphase separation). Different environmental conditions (e.g., solvents) give rise to distinct morphologies. Theoretical techniques^{1,4,14–16} and computer simulations^{18–20} have been used to study how the microphase-separated morphology depends on the incompatibility of the components,^{1,15} solvent selectivity,^{4,14} composition,¹⁵ and chain length asymmetry.¹⁶ Whereas scaling considerations^{1,14} and self-consistent field calculations¹⁵ predict spatially periodic morphologies, simulations^{18–20} and experiments^{4,21,22} observe only structures with poor long-range order. This observation has been traced back to the pronounced amplifications of fluctuations in the local grafting density by microphase separation. Very small fluctuations in the position of the grafting points dictate the location of domains and destroy long-range order, and there are no sharp transitions between different morphologies in a thermodynamic sense.²⁰

Correlations between fluctuations in the grafting-point positions and morphology are difficult to observe directly in experiments. Recent experimental studies, however, introduced a new characteristic called domain memory that quantifies to what extent domains form at the same position and with the same size/shape²² when the morphology of the brush is cyclically changed (e.g., through periodic exposure of the brush to two solvents of different quality).²¹ It was shown that fluctuations in the grafting points act as nucleation centers for the formation of domains.^{21,22} Moreover, the dependence of the memory measure (*mm*) on the chemical structure of the brush (e.g., molecular weight, block

[†] Part of the Stimuli-Responsive Materials: Polymers, Colloids, and Multicomponent Systems special issue.

* Corresponding authors. E-mail: ssanter@imtek.de, mmueller@theorie.physik.uni-goettingen.de.

[‡] University of Freiburg.

[§] University of Tennessee.

^{||} Georg-August Universität.

[⊥] Born Prokhorova.

(1) Marko, J. F.; Witten, T. A. *Phys. Rev. Lett.* **1991**, *66*, 1541. Marko, J. F.; Witten, T. A. *Macromolecules* **1992**, *25*, 296.

(2) Zhulina, E.; Balazs, A. C. *Macromolecules* **1996**, *29*, 2667.

(3) Lin, Y.-H.; Teng, J.; Zubarev, E. R.; Shulha, H.; Tsukruk, V. V. *Nano Lett.* **2005**, *5*, 491.

(4) Minko, S.; Müller, M.; Usov, D.; Scholl, A.; Froeck, C.; Stamm, M. *Phys. Rev. Lett.* **2002**, *88*, 035502.

(5) Zhao, B. *Langmuir* **2004**, *20*, 11748.

(6) Feng, J.; Haasch, R. T.; Dyer, D. J. *Macromolecules* **2004**, *37*, 9525.

(7) Lemieux, M. C.; Julthongpipit, D.; Bergman, K. N.; Cuong, P. D.; Ahn, H.-S.; Lin, Y.-H.; Tsukruk, V. V. *Langmuir* **2004**, *20*, 10046.

(8) Luzinov, I.; Minko, S.; Tsukruk, V. V. *Prog. Polym. Sci.* **2004**, *29*, 635.

(9) Lemieux, M.; Usov, D.; Minko, S.; Stamm, M.; Shulha, H.; Tsukruk, V. V. *Macromolecules* **2003**, *36*, 7244.

(10) Motornov, M.; Minko, S.; Eichhorn, K.-J.; Nitschke, M.; Simon, F.; Stamm, M. *Langmuir* **2003**, *19*, 8077.

(11) Tokarev, I.; Minko, S.; Fendler, J. H.; Hutter, E. *J. Am. Chem. Soc.* **2004**, *126*, 15950.

(12) Tokarev, I.; Krenek, R.; Burkov, Y.; Schmeisser, D.; Sidorenko, A.; Minko, S.; Stamm, M. *Macromolecules* **2005**, *38*, 507.

(13) Draper, J.; Luzinov, I.; Minko, S.; Tokarev, I.; Stamm, M. *Langmuir* **2004**, *20*, 4064.

(14) Singh, C.; Pickett, G. T.; Zhulina, E.; Balazs, A. C. *J. Phys. Chem. B* **1997**, *101*, 10614.

(15) Müller, M. *Phys. Rev. E* **2002**, *65*, 030802(R).

(16) Minko, S.; Luzinov, I.; Luchnikov, V.; Müller, M.; Patil, S.; Stamm, M. *Macromolecules* **2003**, *36*, 7268.

(17) Roan, J. R. *Phys. Rev. Lett.* **2006**, *96*, 248301.

(18) Brown, G.; Chakrabarti, A.; Marko, J. F. *Europhys. Lett.* **1994**, *25*, 239.

(19) Soga, K. G.; Zuckermann, M. J.; Guo, H. *Macromolecules* **1996**, *29*, 1998.

(20) Wenning, L.; Müller, M.; Binder, K. *Europhys. Lett.* **2005**, *71*, 639.

(21) Santer, S.; Kopyshov, A.; Yang, H.-K.; Rühle, J. *Macromolecules* **2006**, *39*, 3056.

(22) Santer, S.; Kopyshov, A.; Donges, J.; Yang, H.-K.; Rühle, J. *Langmuir* **2006**, *22*, 4660.

length, ratio between the (sub-)chain) has been explored.²² The domain memory is of interest for both the fundamental understanding of structure formation in polymer brushes and for applications in nanoscience. As recently demonstrated by some of the authors,^{23–25} mixed polymer brushes can induce motion of nano-objects adsorbed on their top, that is, motion driven by changes in the spatially varying force between brush and particle upon topography switching. If the patterns completely recover their initial conformation after topography switching (complete domain memory), then the brushes are not capable of relocating adsorbed objects. If the domain size and shape are only weakly correlated between subsequent cycles of topography switching, then the brush will induce the motion of adsorbed nano-objects provided some criteria are met, such as compatible surface energies of the object and brush.^{23,24}

Conventionally, mixed brushes are fabricated by first growing one type of polymer via a surface-initiated reaction. The reaction is stopped before all initiator is consumed, and the remaining initiator, which is randomly distributed over the surface, is utilized for the growth of the second type of polymer. Fluctuations in the local density of grafting points of one component can be caused by local variations of the initiator density (density fluctuations) and by local variations of the chemical nature of the attached chains (composition fluctuations). The latter type of fluctuation can be eliminated by using so-called Y initiators that simultaneously anchor both types of polymer chains.

In this work, we investigate how the domain memory measure depends on composition fluctuations of the grafting points by comparing two types of PS–PMMA mixed brushes that are synthesized (i) from a conventional initiator and (ii) from a Y initiator. Our experimental results are compared to single-chain-in-mean-field (SCMF) simulations,^{26–28} and a simple argument for the dependence of the domain memory measure on the grafting density (and concomitant statistical composition fluctuations) is presented. Implications for the transport of nano-objects on such surfaces are discussed.

Experimental Section

Materials and Methods. Y-shaped polystyrene–poly(methyl methacrylate) (PS–PMMA) mixed brushes were prepared from an asymmetric difunctional initiator-terminated self-assembled monolayer (Y-SAM) by combining two different living radical polymerization techniques—atom-transfer radical polymerization (ATRP) and nitroxide-mediated radical polymerization (NMRP).^{29–33} The detailed procedure can be found in a previous publication.²⁹ The Y-SAM was designed to ensure that the two initiators are well mixed on the molecular scale and thus result in good mixing of the two different homopolymers (Scheme 1). PMMA was grown first from the Y-initiator by ATRP at 75 °C, followed by the NMRP of styrene at 115 °C. Corresponding free initiators were added to the reaction mixtures to control the polymerization. We confirmed that the molecular weights and molecular weight distributions of grafted polymers were essentially identical to those of free polymers.³² Although we do not know exactly how many PMMA chains are

Scheme 1. Synthesis of Y-shaped PS–PMMA Mixed Brushes from Y-SAM

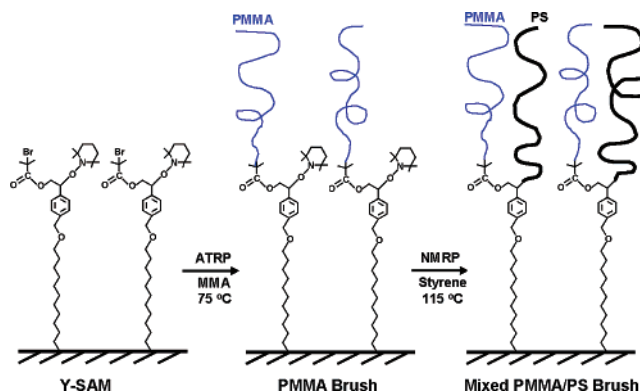


Table 1. Molecular Parameters of Y-Shaped PS–PMMA Mixed Brushes

	M_n^{PMMA} g/mol ^a	σ^{PMMA} chains/nm ²	h^{PMMA} nm ^b	M_n^{PS} g/mol ^a	σ^{total} chains/nm ²	h^{total} nm ^b
Y-I	2.3×10^4	0.59	19	1.8×10^4	1.01	31
Y-II	2.3×10^4	0.59	19	2.1×10^4	1.01	33
Y-III	2.5×10^4	0.56	19.5	2.1×10^4	1.00	34

^a The number-average molecular weights of free PS and PMMA were measured by GPC in THF versus PS and PMMA standards with a narrow polydispersity. ^b The thicknesses of PMMA brushes and PS–PMMA mixed brushes were measured by ellipsometry using a refractive index of 1.49.

covalently bound to PS chains through the Y junction, the GPC analysis of the polymer that was cleaved from the mixed brush-grafted silica nanoparticles indicates that a significant portion of the mixture was the degrafted diblock copolymer grown from the Y-initiator molecule.³²

Three samples of Y-shaped mixed brushes are used in this study, and the molecular parameters are summarized in Table 1. The thickness of the PMMA brush after ATRP was ~ 19 nm for all three samples, and the total dry thicknesses of brushes I, II, and III are 31, 33, and 34 nm, respectively. Calculations show that the PMMA grafting density is 0.59 chains/nm² in brushes I and II and 0.56 chains/nm² for brush III. The total grafting density is ~ 1.01 chains/nm² for the three samples. This implies that some initiators in the Y-SAM were not activated during the synthesis of polymer brushes.

The conventional polystyrene–poly(methyl methacrylate) (PS–PMMA) mixed brushes were synthesized using surface-initiated radical polymerization as described elsewhere.^{34–37} PS chains were first grown from the azo initiator attached to a silicon wafer, followed by growing the PMMA chains (Scheme 2).²¹

Three PS–PMMA mixed brushes with a fixed grafting density of $\sigma = 0.06$ chains/nm² and a molecular weight of the PS chains of $M_n^{\text{PS}} = 3 \times 10^5$ g/mol were studied, differing in molecular weight of the PMMA chains, which ranges from 3×10^5 to 1×10^6 g/mol (Table 2). The total dry thickness of the brush varies accordingly from 25 nm to 34 nm.^{21,22}

Instrumentation. An atomic force microscope (AFM) (Multi-Mode, Veeco Metrology Group) was used to characterize the morphology of the layers. Tapping mode images were acquired using silicon cantilevers (Olympus) with a resonance frequency of ~ 300 kHz, a spring constant of ~ 50 N/m, and a tip radius of ~ 10 nm. For pumping the solvents, we designed a system with a mechanical pump that connects two reservoirs—one filled with acetone the other with toluene—and has an inlet for dry, clean air. With an appropriate switch, it was possible to control the flow of

(23) Santer (Prokhorova), S. A.; Rhe, J. *Polymer* **2004**, *45*, 8279.

(24) Prokhorova, S. A.; Kopyshv, A.; Ramakrishnan, A.; Zhang, H.; Rhe, J. *Nanotechnology* **2003**, *14*, 1098.

(25) Santer, S.; Kopyshv, A.; Donges, J.; Yang, H.-K.; Rhe, J. *Adv. Mater.* **2006**, *18*, 2359.

(26) Mller, M.; Smith, G. D. *J. Polym. Sci., Part B: Polym. Phys.* **2005**, *43*, 934.

(27) Daoulas, K. Ch.; Mller, M.; Nealey, P. F.; de Pablo, J. J.; Smith, G. D. *Soft Matter* **2006**, *2*, 573.

(28) Daoulas, K. Ch.; Mller, M. *J. Chem. Phys.* **2006**, *125*, 184904.

(29) Zhao, B.; He, T. *Macromolecules* **2003**, *36*, 8599.

(30) Zhao, B.; Haasch, R. T.; MacLaren, S. *J. Am. Chem. Soc.* **2004**, *126*, 6124.

(31) Zhao, B.; Zhu, L. *J. Am. Chem. Soc.* **2006**, *128*, 4574.

(32) Li, D.; Sheng, X.; Zhao, B. *J. Am. Chem. Soc.* **2005**, *127*, 6248.

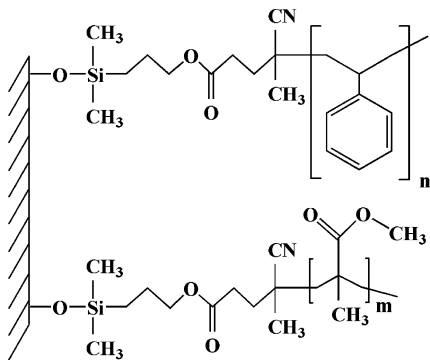
(33) Zhao, B.; Haasch, R. T.; MacLaren, S. *Polymer* **2004**, *45*, 7979.

(34) Prucker, O.; Rhe, J. *Macromolecules* **1998**, *31*, 592.

(35) Prucker, O.; Rhe, J. *Langmuir* **1998**, *14*, 6893.

(36) Prucker, O.; Rhe, J. *Macromolecules* **1998**, *31*, 602.

(37) Schimmel, M. Ph.D. Dissertation, MPI for Polymer Research, Mainz, Germany, 1998.

Scheme 2. Chemical Structure of the Conventional PS–PMMA Mixed Brush**Table 2. Molecular Parameters of Conventional PS–PMMA Mixed Brushes**

	M_n^{PS} g/mol ^a	σ^{PS} nm ⁻²	h^{PS} nm ^b	M_n^{PMMA} g/mol ^a	σ^{total} nm ⁻²	h^{total} nm ^b
I	3×10^5	0.042	20	0.3×10^6	0.06	25
II	3×10^5	0.042	20	0.5×10^6	0.06	30
III	3×10^5	0.042	20	1×10^6	0.06	34

^a The number-average molecular weights of the free PS and PMMA polymers were measured using an Agilent GPC setup. ^b The thickness of the brushes was measured in the dry state using an ELX-1 ellipsometer (Riss, Germany) operating with a 632.8 nm He/Ne laser at an incident angle of 70°. The refractive index of PMMA was assumed to be 1.49. The refractive index of the mixed layer (PMMA and PS) was calculated from a linear combination of the two refractive indices.

solvents or vapor through the AFM cell. After solvent exposure, the samples were typically dried in air for 2 min. The AFM images were recorded in air at a relative humidity of 40–45% and at room temperature (25 °C). During solvent pumping, image acquisition was stopped without withdrawing the tip, allowing us to obtain an image of the same area on the brush while switching the solvent and thus the topography.

For the calculation of the cross-correlation function describing the similarity of two images, image-processing software was developed on the basis of commercial PV-Wave software.²² The covariance of the brightness distribution of AFM micrographs taken at two subsequent switching cycles was calculated as described elsewhere.²² The measure of correlation between two images is characterized by the absolute value of covar and is termed the memory measure (mm). The case of $mm = 1$ corresponds to the absolute domain memory of the brush domains (i.e., the domains appear at exactly the same position and with exactly the same shape as in the previous switching cycle). A lower value of mm indicates a weaker memory of the brush domains.

To calculate the covariance of a certain brush, areas of (1.5 μm)² from at least 10 different spots on the brush were examined, and the covariances were averaged over switching cycles at the same spot and between different spots on the brush. Thus, the covariance reflects the characteristics of the whole sample.

Single-Chain-in-Mean-Field (SCMF) Simulations.^{26–28} We study microphase separation in mixed polymer brushes within the framework of a coarse-grained polymer model. This minimal model is characterized by a small number of coarse-grained parameters—the end-to-end distance of the ungrafted chains in the molten state, R_e , and the incompatibility between chains of different types, χN . The chain conformations are described by a discretized Edwards Hamiltonian

$$\frac{H_b[r(s)]}{k_B T} = \sum_{s=1}^{N-1} \frac{3(N-1)}{2R_{e0}^2} [r_i(s) - r_i(s+1)]^2 \quad (1)$$

where R_e^2 denotes the mean square end-to-end distance of the polymers in a dense melt. This is the only characteristics of a Gaussian

Table 3. Parameters of SCMF Simulations^a

system	brush height D/R_e	number of chains $n_A = n_B$
small	1	8192
medium (R/Y)	1	16 384
large	1	32 768
H2	2	16 384

^a Incompatibility, $\chi N = 30$; inverse compressibility, $\kappa N = 50$; chain discretization, $N = 32$; spatial discretization, $\Delta L = R_e/6$; and lateral system size, $L = 16R_e$ for all systems.

chain, and R_e sets the unit length scale. The chain contour of both species is discretized into $N = 32$ effective segments and space into cells of linear extent, $\Delta L = R_e/6$. For simplicity, we assume that both components of the mixed brush have equal size, R_e . The relevant nonbonded interactions consist of the excluded volume of the effective segments and the repulsion between unlike segment species that gives rise to microphase separation.

$$\frac{H_{\text{nb}}[\phi_A, \phi_B]}{k_B T} = \frac{\rho}{N} \int_V d^3r \left(\frac{\kappa N}{2} [\phi_A + \phi_B - 1]^2 - \frac{\chi N}{4} [\phi_A - \phi_B]^2 \right) \quad (2)$$

where $\rho \equiv (n_A + n_B)N/DL^2$ denotes the segment number density and

$$\phi_A(r) = \frac{1}{\rho} \sum_{i=1}^{n_A} \sum_{s=1}^N \delta(r - r_i(s)) \quad (3)$$

is the microscopic local A density. A similar expression holds for ϕ_B . The excluded volume interactions of the effective segments are modeled via a Helfand compressibility term that penalizes fluctuations of the local density from its average. κ describes the inverse thermal compressibility of the segment fluid. The repulsion between unlike segments is parametrized by a Flory–Huggins parameter, χ . In our numerical calculations, we utilize the values $\chi N = 30$ and $\kappa N = 50$. This gives rise to well-segregated domains and only small density fluctuations.

The partition function of the mixed polymer brush is given by

$$Z \sim \int \prod_{i=1}^{n_A+n_B} D[r_i(s)] \exp\left(-\frac{H_b[r_i(s)] + H_{\text{nb}}[\phi_A, \phi_B]}{k_B T}\right) \quad (4)$$

where D sums over all conformations of n_A molecules of type A and n_B molecules of type B. The grafting points are irreversibly attached to the substrate at $z = 0$ and their lateral position is fixed. The distribution of grafting points is completely random. The grafting density is given by $\sigma \equiv (n_A + n_B)/L^2$. We model Y-shaped initiators by choosing the same grafting points for A and B molecules. Both the grafting surfaces and the liquid–vapor (vacuum) interface of the brush are modeled by non-penetrable, hard walls at $z = 0$ and D that exhibit no preference for species A or B. The lateral system size is L , and periodic boundary conditions are applied in the x and y directions. The system parameters are compiled in Table 3.

Microphase separation is studied by SCMF simulations,^{26–28} which is a particle-based self-consistent field scheme that allows us to investigate the structure formation in large 3D systems. For each set of parameters, 32 independent systems with an identical distribution of grafting points have been simulated. The starting configuration consists of random, disordered morphology that corresponds to $\chi N = 0$. The independent systems are quenched to $\chi N = 30$. Local displacements segments are utilized to update the molecular conformations.

The evolution of the morphology after such a quench is presented in Figure 1. A microphase-separated structure has formed after 32 000 attempted local random segment displacements per segment (MCS). After this stage, the morphology evolves very slowly. We analyze the structure of the different systems after $(1-4) \times 10^5$ MCS, which yields a good approximation for the equilibrium properties.

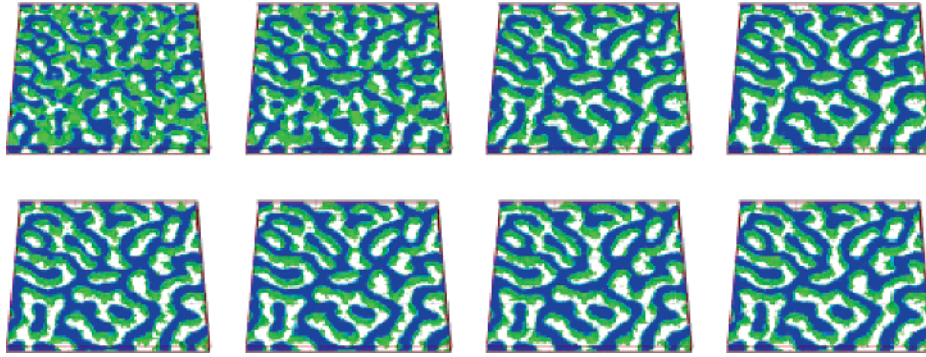


Figure 1. Evolution of the microphase-separated morphology after a quench from the disordered phase to $\chi N = 30$. The configuration consists of a randomly mixed polymer brush with $n_A = n_B = 16\,384$ (i.e., $\sigma R_e^2 = 128$). The A component is removed, and the B component is blue shaded. The AB interface between domains is depicted in green. Configurations after 4000, 8000, 16 000, 32 000, 64 000, 128 000, 256 000, and 512 000 MCS are presented. The lateral system size is $L = 16R_e$, and the brush height is $D = 1R_e$.

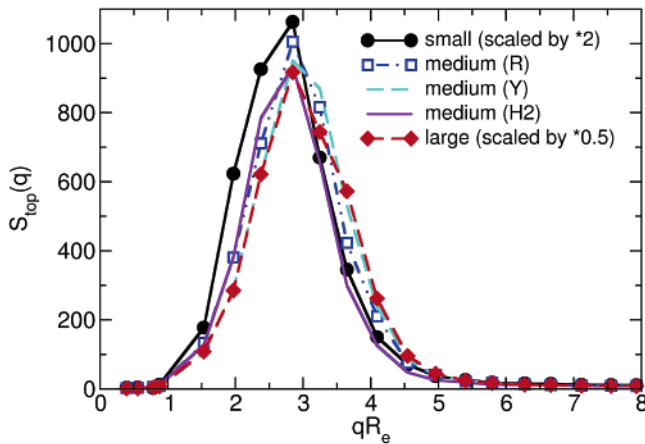


Figure 2. Structure factor of composition fluctuations of the final morphology calculated from the top 25% of the brush for the different grafting schemes.

The type of grafting, the grafting density, and the brush height have only a minor influence on the disordered morphology of the brush. In Figure 2 we present the circularly averaged structure factor, $S_{\text{top}}(q)$, of composition fluctuations. Only the top quarter of the brush has been utilized to calculate $S_{\text{top}}(q)$. The domain size, determined from the peak of the 2D structure factor of composition fluctuations, is $\lambda \approx 2.2R_e$. It slightly increases as we reduce the grafting density and thereby increase the fluctuations of the grafting points. Other properties, such as the Euler characteristics of the 2D morphology on the top of the brush, are very similar for the different brushes.

To analyze the structure on the top of the brush, we average the composition, $\phi = \rho_A/(\rho_A + \rho_B)$, over patches of lateral size $\Delta L = R_e/6$ and consider all segments with $(D - R_e)/6 \leq z \leq D$. For each system, $f = 1, \dots, 32$ of lateral extent $L = 16R_e$. This procedure yields a composition array $\phi_f(i_x, j_y)$ of size 96×96 . Correlating the normalized local composition, $\delta\phi_f(i_x, j_x) = \phi_f(i_x, j_x) - (\Delta L/L)^2 \sum_{i_x, j_x} \phi_f(i_x, j_x)$, of independent systems with identical locations of the grafting points, we mimic the experimental procedure and obtain

$$\text{corr}(\delta_x, \delta_y) \equiv \left\langle \frac{\sum_{i_x, j_y} \delta\phi_f(i_x, j_y) \delta\phi_g(i_x + \delta_x, j_y + \delta_y)}{\sqrt{\sum_{i_x, j_y} \delta\phi_f^2(i_x, j_y) \sum_{i_x, j_y} \delta\phi_g^2(i_x + \delta_x, j_y + \delta_y)}} \right\rangle \quad (5)$$

where the average $\langle \dots \rangle$ runs over all pairs (f, g) of independent configurations. In the simulations, we know the exact location of the grafting points and therefore can correlate morphologies that form on top of identical patches. This correlations is given by $m^* \equiv \text{corr}(\delta_x = 0, \delta_y = 0)$. In the experiment it is not possible to find

exactly the same location after different solvent exposures, thus one maximizes the domain memory measure by allowing for a local shift (δ_x, δ_y) of the two patches that are correlated with each other. In the analysis of the simulation data, we can also mimic this procedure and evaluate

$$mm \equiv \max_{\delta_x, \delta_y} \text{corr}(\delta_x, \delta_y) \quad (6)$$

Figure 3a investigates the dependence of the domain memory measure on the area of the subsystem (patch) that is utilized to correlate independent morphologies. If one correlates morphologies with identical distribution of grafting points, then the domain memory measure, m^* , will slightly increase for very small patch sizes but will rapidly approach a limiting value for lateral patch sizes that are large than $4R_e \approx 2\lambda$. Because our simulation cell exceeds this value by a factor of 4, we do not expect our results be affected by finite size effects. When we maximize $m(\delta_x, \delta_y)$ with respect to the relative shift of the patch location (and therefore the position of the grafting points), however, we observe a rather pronounced decrease in mm with the lateral patch size, and only for very large systems do we recover the value of m^* . This size dependence does not directly characterize the correlation between the morphology and distribution of grafting points, but rather it provides information about how large a patch is required to identify it accurately. The data indicate that one needs patches of a linear extension of 5λ to identify a location. In the inset of Figure 3a, we present the average misalignment, $\delta x^2 = \delta_x^2 + \delta_y^2$, as a function of the area of the patch or the number of domains, respectively, and find an inverse relationship.

The dependence of the memory measure on the lateral patch size in the experiment is shown in Figure 3b. The size of the micrographs at which mm levels off in the experiment, however, is significantly larger than in the simulations. For a conventional brush (back squares), patches of about 10λ are required to observe a size-independent value whereas in the case of Y-shaped brushes asymptotic behavior is attained only for micrographs of linear dimension 50λ . This surprisingly large value as well as the larger asymptotic value of the memory measure may indicate weak but long-range density fluctuations in the grafting points. In this article, only mm values from an area larger than $1.5 \mu\text{m}$ are discussed.

Results and Discussions

One experimentally accessible way of controlling fluctuations of the grafting density consists of varying the invariant grafting density, σR_e^2 , by either increasing the molecular weight of the polymers, $R_e^2 \sim M_w$, or increasing the area density, σ , of grafting sites. Because the characteristic size, λ , of the domains is proportional to R_e , the average number of molecules in one domain scales like σR_e^2 . If the grafting occurs randomly, then the fluctuation of the number of chains in a patch of size $\lambda \sim R_e^2$ will be proportional to $\Delta\phi_g \sim 1/\sqrt{\sigma R_e^2}$. Thus, the fluctuations of the composition of the grafting points inside a domain of typical size

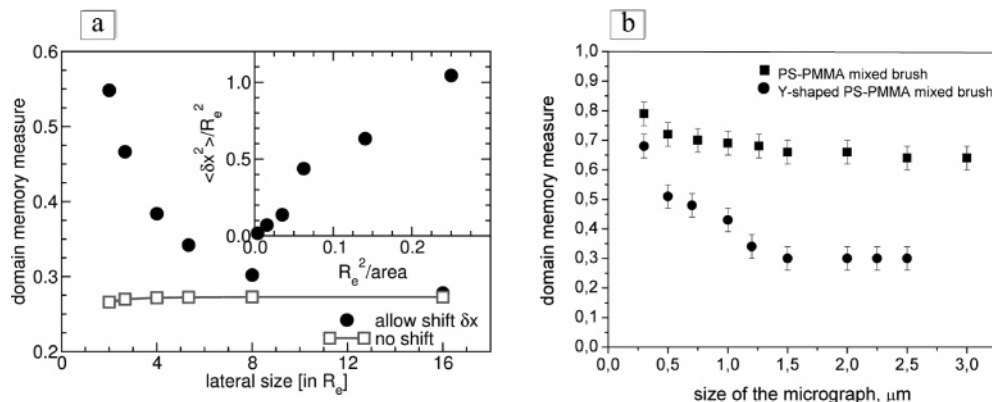


Figure 3. (a) Dependence of the domain memory measures, m^* and mm , on the lateral patch size for a conventional brush (medium, R). m^* hardly exhibits a dependence on the lateral extent. mm , however, decreases with the area of the patches that are correlated, and only for rather large lateral sizes do m^* and mm agree. The inset displays the mean squared average shift $\delta x^2 = \delta_x^2 + \delta_y^2$ as a function of the inverse area of the patch. (b) Dependence of the domain memory measure, mm , on the size of the micrographs as measured from AFM experiments. The chain extensions in the experiment are $R_e \approx 0.04$ and $0.01 \mu\text{m}$ for the conventional and Y-shaped brushes, respectively.

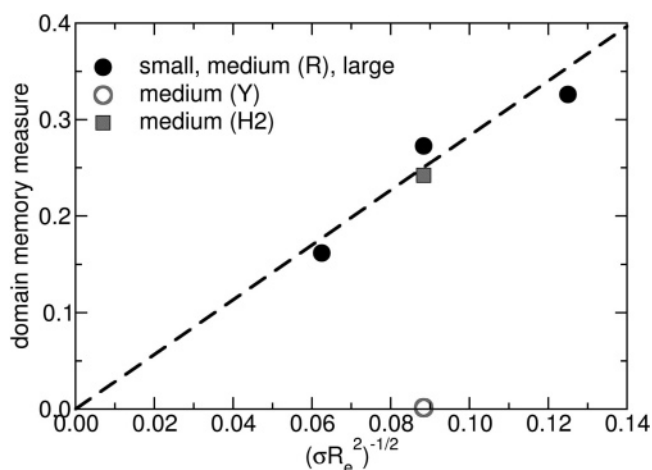


Figure 4. Dependence of the domain memory measure on the grafting scheme in SCMF simulations.

are given by $\sqrt{\sigma R_e^2}$. If the amplitude, $\Delta\phi_g \sim 1/\sqrt{\sigma R_e^2}$, of this fluctuation of the grafting points is sufficiently large, then it will template a domain of the corresponding species in the brush. Because the memory measure quantifies the density of corresponding domains in systems with identical grafting points, we expect it to be proportional to $\Delta\phi_g$, thus $mm \sim 1/\sqrt{\sigma R_e^2}$.

The dependence of the memory measure extracted from SCMF simulations is shown in Figure 4. Indeed, we find that $mm \sim 1/\sqrt{\sigma R_e^2}$. Note that the thickness of the brush, D , does not significantly influence the domain memory, as can be observed by comparing brushes with height $D = R_e$ and $2R_e$ but with an identical number of grafted chains. The graph also displays the result for the Y-shaped brush. Because there is one A and one B chain attached to every grafting point, there are no composition fluctuations (only density fluctuations), and the concomitant domain memory measure is very small.

In the experiment, we investigate the structure formation in two types of polystyrene–poly(methyl methacrylate) (PS–PMMA) mixed brushes: (1) those synthesized from an azo initiator by surface-initiated radical polymerization (Scheme 2, Figure 5a) and (2) those grown from a Y-shaped initiator using combination of ATRP and NMRP (Scheme 1, Figure 5b). In addition, the chain length of one species is varied (Figure 5).

Depending on the solvent to which the brush is exposed, the topography of both types of brushes can adopt a flat, laterally homogeneous state or a laterally microphase-separated morphol-

ogy.^{21,22} In the experiment, we cyclically expose the mixed brushes to acetone and toluene solvents and thereby switch from a laterally structured state to flat morphology back and forth. It was shown that exposing the brushes to the corresponding solvents only for 10 s was sufficient to switch their topography between the structured and the flat state.^{21,22} Increasing the exposure time up to 10 min did not alter the shape of the pattern formed or the value of the memory measure.^{21,22} In the present experiments, the exposure time was kept as short as possible.

Figures 6 and 7 show the AFM micrographs of the I-Y-shaped and II-Y-shaped PS–PMMA mixed brushes after the first and second cycles of topography switching. In both cases, a weak domain memory effect can be observed even visually by comparing characteristic features such as a region resembling the letter A or a “heart” in the micrographs of Figures 6 and 7.

The characteristic size of the pattern is much smaller than in the case of a conventional PS–PMMA mixed brush. In the latter case, the distance between two neighboring domains is 120 nm for brush I with $M_n^{\text{PMMA}} = 3 \times 10^5 \text{ g/mol}$, whereas in the case of Y-shaped PS–PMMA mixed brush II with $M_n^{\text{PMMA}} = 2.3 \times 10^4 \text{ g/mol}$ the pattern size is 27 nm. Much of this difference is due to the different molecular weights. Using the relationship $R_e^{\text{PMMA}} = (0.576M_w^{0.98})^{1/2} \text{ \AA}$ ³⁸ or a statistical segment length of 0.7 nm,³⁹ one obtains end-to-end distances of $R_e \approx 38$ and 11 nm and domains of $3.15R_e$ and $2.45R_e$ for the conventional and Y-shaped brushes, respectively. The fact that even the rescaled domain spacing is larger in the experiment than in the simulations may partially be explained by additional fluctuations in the grafting points (density fluctuations or imperfections in the Y brush) that are not modeled in the simulations. These fluctuations tend to increase the spacing (Figure 2) and also result in a larger domain memory in the experiment.

As a consequence of the distribution of grafting points, the brush topography partially restores its local composition and pattern on the nanometer scale after treatment with appropriate solvents. Figure 8 shows that the memory measure changes from 0.73 ± 0.04 to 0.65 ± 0.04 to 0.53 ± 0.04 for conventional brushes I, II, and III (Table 2), respectively. In the case of Y-shaped mixed brushes, where the two chains (PS and PMMA) are grown from the same grafting point (Y-SAM) (Table 1), the domain memory measure is significantly reduced. This is in accord with the reduced composition fluctuations of the grafting points. The

(38) Kirste, R. G.; Kruse, W. A.; Ibel, K. *Polymer* **1975**, *16*, 120.

(39) Sferazza, M.; Xiao, C.; Bucknall, D. G.; Jones, R. A. L. *J. Phys. Condens. Matter* **2001**, *13*, 10269.

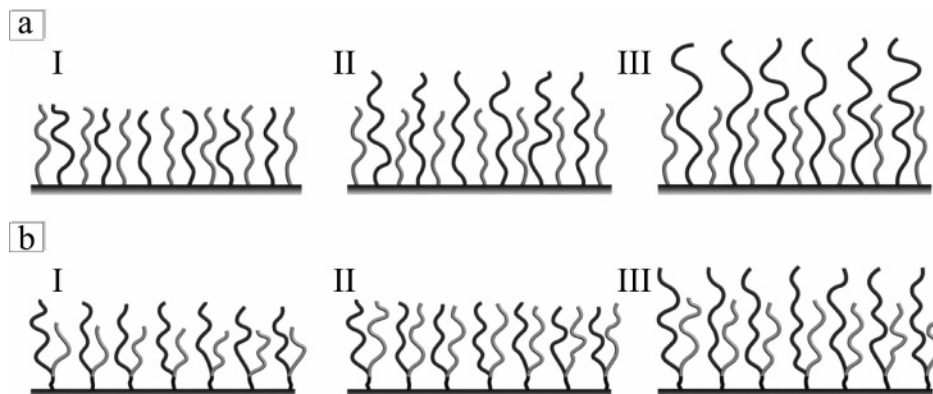


Figure 5. Schematic representation of two types of PS-PMMA mixed brushes. PMMA and PS chains are shown in black and gray, respectively. (a) Conventional PS-PMMA mixed brushes with a fixed grafting density and molecular weight of the PS chains and differing in the length of the PMMA chains, resulting in ratio $\phi = M_n^{\text{PMMA}}/M_n^{\text{PS}}$ of 1, 1.67, and 3.33 for brushes I, II, and III, respectively (Table 2).^{21,22} (b) Y-shaped PS-PMMA mixed brushes with the same grafting density but differing in the ratio $\phi = M_n^{\text{PS}}/M_n^{\text{PMMA}}$, with values of 0.78, 0.91, and 0.84 for I-Y, II-Y, and III-Y, respectively (Table 1).

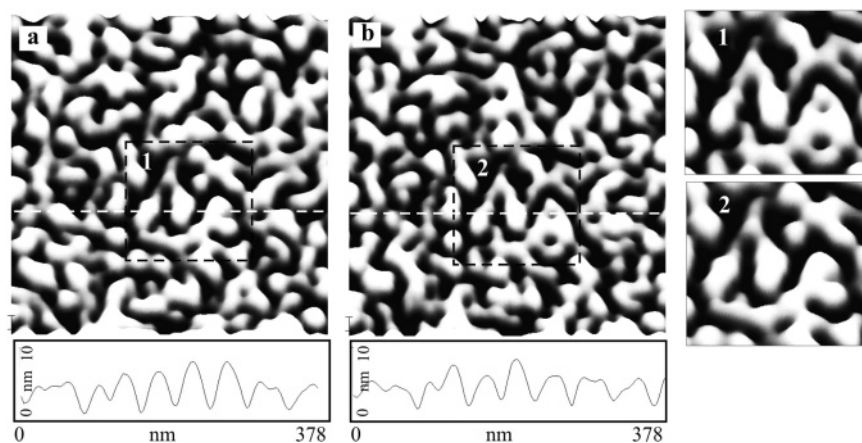


Figure 6. AFM micrographs of brush I-Y (Table 1) recorded after acetone treatment (a) before topography switching to the flat state and (b) after one cycle of topography switching. The topography is turned to the patterned state shown in the micrographs by treating the brush with acetone, which is a better solvent for PMMA than for PS. The flat state is produced by exposing the brush to toluene solvent, which is a good solvent for both polymers. The cross section along the line cut (white dashed line) is shown beneath. In the micrographs, two areas marked 1 and 2 are selected, and close-ups of these regions are shown on the right-hand side.

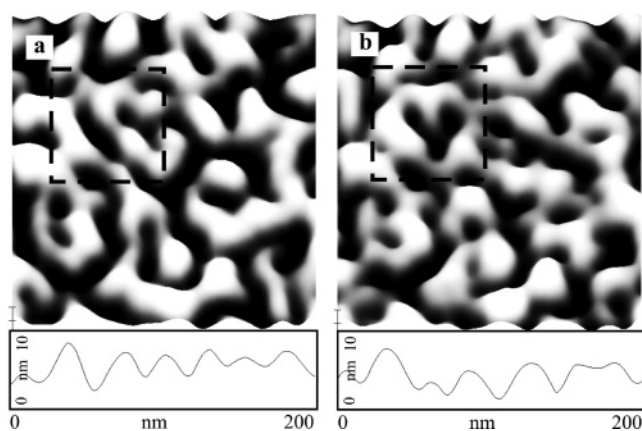


Figure 7. AFM micrographs of brush II-Y acquired after the first cycle (a) and the second cycle (b) of exposure to acetone/toluene/acetone solvents. The cross section over the "heart" pattern marked by the dashed black square is shown at the bottom of the micrographs.

memory measure, mm , differs by roughly a factor of 2 when comparing the Y-shaped brush (II) to the conventional brush (I) at similar ϕ ($mm = 0.30 \pm 0.04$ and 0.73 ± 0.04 , respectively). The parameter ϕ is calculated as the ratio of the molecular weight of the block varied in the experiments to the weight of the other block, which is held constant. Thus, we have $\phi = M_n^{\text{PS}}/M_n^{\text{PMMA}}$

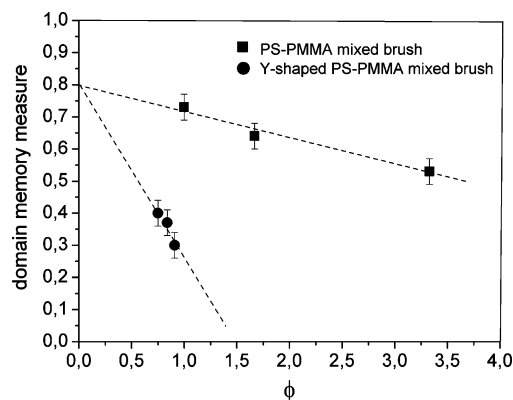


Figure 8. Dependence of the memory measure, mm , on the ratio ϕ for two types of brushes: black squares and circles indicate conventional and Y-shaped PS-PMMA mixed brushes, respectively.

in the case of Y-shaped mixed brushes, and $\phi = M_n^{\text{PMMA}}/M_n^{\text{PS}}$ for the conventional mixed brushes. This distinction becomes necessary because the first block dictates the distribution of possible nucleation centers and stays constant through the corresponding series of the brushes, whereas for the vanishing weight of the second block the mm should always attain a maximum value characteristic of homopolymer brushes. Then, as expected, the memory measure of the Y-shaped mixed brushes

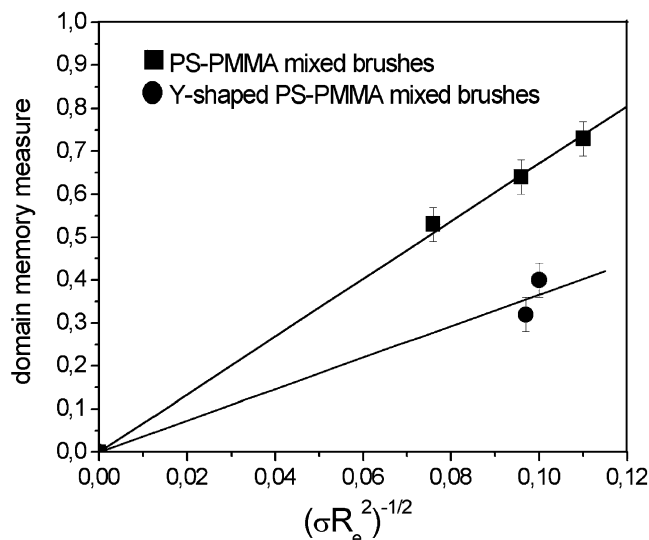


Figure 9. Dependence of the memory measure of conventional PS–PMMA mixed brushes (black squares) and Y-shaped PS–PMMA mixed brushes (black circles) on $\Delta\phi_g \sim 1/\sqrt{\sigma R_e^2}$.

decreases with the appropriately defined ϕ just as in the case of conventional mixed brushes (Figure 8) and extrapolates to the same value for $\phi = 0$, $mm = 0.79$, which is similar in order of magnitude to the value of 0.8 obtained from the Monte Carlo simulations of one-component homopolymer brushes.²⁰

Figure 9 displays the dependence of mm over $mm \sim 1/\sqrt{\sigma R_e^2}$ for two types of PS–PMMA mixed brushes. (The III-Y brush is not included because it was synthesized in a different batch, giving rise to a slightly different grafting density.) The variation in chain length asymmetry present in the experiments is not directly accessible as an input to the simulations, but both experimental and simulation data (Figures 4 and 9) are in excellent agreement with respect to the linear dependence of the domain memory measure on $\Delta\phi_g \sim 1/\sqrt{\sigma R_e^2}$. When quantitatively comparing to the simulation results (Figure 4), we note, however, that the domain memory effect is larger in the experiment than in the simulation and also the reduction of mm in Y-shaped brushes is smaller.

There are several explanations for this discrepancy: (i) the segregation in the simulation might be different than in the experiment. (ii) The Y-shaped mixed brushes used in the present study are not perfect but contain a small fraction of singly grafted chains. This explanation is supported by the small but non-negligible difference between the grafting densities of the two polymer chains. Moreover, the density distribution in the

experiment may be not perfectly random as assumed in the simulations. (iii) Although not evident from AFM micrographs (see discussion above), the time between exchanging the solvents may not have been sufficiently long to erase deeper-lying phase-separated structures completely (i.e., the morphology is close to that of the grafting substrate⁴⁰). (iv) In the laterally segregated state, one component may exhibit a small preference for the substrate or the interface with the vapor. This selectivity is not considered in the SCMF simulations. Note also that the experiment monitors the topography whereas the simulations study the composition at the flat top surface of the brush. In view of these differences, only qualitative agreement between experiment and simulation can be expected.

Conclusions

The dependence of the domain memory on the grafting scheme has been investigated by comparing two types of mixed brushes: (i) conventional and (ii) Y-shaped. In the case of conventional mixed brushes, there are significant fluctuations in both the grafting density and local composition of the attached chains. Composition fluctuations of the grafted chains result in a strong domain memory effect (i.e., there is a high probability that a specific domain re-forms at the same position and with the same shape after switching the morphology from a laterally structured to a laterally homogeneous one back and forth). Y-shaped PS–PMMA mixed brushes, in contrast, exhibit a significantly weaker domain memory because fluctuations in the composition of the grafting points are eliminated. This feature is born out both by the SCMF simulations and experiments and demonstrates the importance of local fluctuations in the positions of the grafting points for the nucleation of the domain structure in mixed polymer brushes. The results also exemplify how to control these quenched fluctuations during the synthesis of the brush.

The domain memory measure of brushes is an important characteristic of mixed polymer brushes because it dictates the ability of mixed brushes to relocate nano-objects upon morphology switching. Our results indicate that Y-shaped mixed brushes are particularly promising candidates for pursuing this type of application.

Acknowledgment. It is a pleasure to thank K. Ch. Daoulas for enjoyable and fruitful discussions. Financial support was provided by the DFG under grants Mu1674/3-2, Mu1674/4-1, and PR715/1-2 and the Landesstiftung Baden-Württemberg (Germany). The calculations were performed at the John von Neumann Institute for Computing, Jülich, Germany.

LA0629577

(40) Ruths, M.; Johannsmann, D.; Ruhe, J.; Knoll, W. *Macromolecules* **2000**, *33*, 3860.